

# Mapping the dynamics of a giant Ly $\alpha$ halo at $z = 4.1$ with MUSE: the energetics of a large-scale AGN-driven outflow around a massive, high-redshift galaxy

A. M. Swinbank,<sup>1\*</sup> J. D. R. Vernet,<sup>2</sup> Ian Smail,<sup>1</sup> C. De Breuck,<sup>2</sup> R. Bacon,<sup>3</sup> T. Contini,<sup>4</sup> J. Richard,<sup>3</sup> H. J. A. Röttgering,<sup>5</sup> T. Urrutia<sup>6</sup> and B. Venemans<sup>7</sup>

<sup>1</sup>*Institute for Computational Cosmology, Durham University, South Road, Durham DH1 3LE, UK*

<sup>2</sup>*European Southern Observatory, Karl Schwarzschild Straße 2, D-85748 Garching, Germany*

<sup>3</sup>*CRAL, Observatoire de Lyon, Université Lyon 1, 9 Avenue Ch. Andre, F-69561 Saint Genis Laval Cedex, France*

<sup>4</sup>*Dipartimento di Fisica e Astronomia, University of Padova, Vicolo dell'Osservatorio 2, I-35133 Padova, Italy*

<sup>5</sup>*Leiden Observatory, Leiden University, PO Box 9513, NL-2300 RA Leiden, the Netherlands*

<sup>6</sup>*Leibniz Institut für Astrophysik, An der Sternwarte 16, D-14482 Potsdam, Germany*

<sup>7</sup>*Max-Planck Institut für Astronomie, Königstuhl 17, D-69117 Heidelberg, Germany*

Accepted 2015 February 18. Received 2015 February 18; in original form 2015 January 20

## ABSTRACT

We present Multi Unit Spectroscopic Explorer (MUSE) integral field unit spectroscopic observations of the  $\sim 150$  kpc Ly $\alpha$  halo around the  $z = 4.1$  radio galaxy TN J1338–1942. This 9-h observation maps the full two-dimensional kinematics of the Ly $\alpha$  emission across the halo, which shows a velocity gradient of  $\Delta v \sim 700$  km s $^{-1}$  across 150 kpc in projection, and also identified two absorption systems associated with the Ly $\alpha$  emission from the radio galaxy. Both absorbers have high covering fractions ( $\sim 1$ ) spanning the full  $\sim 150 \times 80$  kpc $^2$  extent of the halo. The stronger and more blueshifted absorber ( $\Delta v \sim -1200$  km s $^{-1}$  from the systemic) has dynamics that mirror that of the underlying halo emission and we suggest that this high column material ( $n(\text{H I}) \sim 10^{19.4}$  cm $^{-2}$ ), which is also seen in C IV absorption, represents an outflowing shell that has been driven by the active galactic nuclei (AGN) or the star formation within the galaxy. The weaker ( $n(\text{H I}) \sim 10^{14}$  cm $^{-2}$ ) and less blueshifted ( $\Delta v \sim -500$  km s $^{-1}$ ) absorber most likely represents material in the cavity between the outflowing shell and the Ly $\alpha$  halo. We estimate that the mass in the shell must be  $\sim 10^{10} M_{\odot}$  – a significant fraction of the interstellar medium from a galaxy at  $z = 4$ . The large scales of these coherent structures illustrate the potentially powerful influence of AGN feedback on the distribution and energetics of material in their surroundings. Indeed, the discovery of high-velocity ( $\sim 1000$  km s $^{-1}$ ), group-halo-scale (i.e.  $> 150$  kpc) and mass-loaded winds in the vicinity of the central radio source is in agreement with the requirements of models that invoke AGN-driven outflows to regulate star formation and black hole growth in massive galaxies.

**Key words:** galaxies: evolution – galaxies: high-redshift.

## 1 INTRODUCTION

Theoretical models of galaxy formation are increasingly successful in their ability to predict the observed properties of galaxies across cosmic time. The most successful models invoke a dramatic form of energy injection from the central active galactic nuclei (AGN) and from star formation and supernovae to drive high-velocity (100s km s $^{-1}$ ), galaxy-wide (i.e.  $\gg 10$  kpc) and mass-loaded energetic outflows. These winds expel significant amounts of gas from the host galaxy and consequently this shuts down future star for-

mation and black hole growth. This process should also enrich the larger scale environment with metals (e.g. Silk & Rees 1998; Fabian 1999; Benson et al. 2003; Springel & Hernquist 2003; Granato et al. 2004; Di Matteo, Springel & Hernquist 2005; Springel, Di Matteo & Hernquist 2005; Hopkins et al. 2006, 2008; Booth & Schaye 2010; Debuhr, Quataert & Ma 2012). In the models, this feedback mechanism is required to prevent the runaway cooling of gas in massive haloes and so match the galaxy luminosity function at  $z = 0$  (e.g. Bower et al. 2006; Croton et al. 2006).

If this feedback mechanism is the dominant route by which massive galaxies terminate their star formation, then it is critical that the AGN feedback is at its maximum efficiency at the epoch where the bulk of the stars in the most luminous elliptical galaxies appear

\* E-mail: [a.m.swinbank@durham.ac.uk](mailto:a.m.swinbank@durham.ac.uk)

to be formed,  $z > 3\text{--}5$  (Nelan et al. 2005). This is therefore the era to search for evidence of AGN feedback in massive galaxies. High-redshift radio galaxies are one potential laboratory to search for evidence of this feedback ‘in action’, as they appear to be amongst the most evolved and most massive galaxies in the early Universe, host energetic AGN and have the properties expected for the progenitors of today’s central cluster galaxies (De Breuck et al. 2002).

Potential evidence for such ‘AGN feedback’ may come from the discovery of much extended Ly $\alpha$  haloes with spatial extents of  $\sim 100\text{--}200$  kpc which are being found in increasing numbers in the high-redshift Universe, including around high-redshift radio galaxies (van Ojik et al. 1997; Venemans et al. 2007). Many of these appear to be associated with young, massive galaxies which display high levels of starburst and AGN activity (e.g. van Breugel et al. 1998; Matsuda et al. 2011). One simple interpretation is that these Ly $\alpha$  haloes represent gas reservoirs which are being ionized by ultraviolet (UV) emission, shocks and outflows from the active galaxies within the haloes (e.g. Taniguchi, Shioya & Kakazu 2001; Geach et al. 2009; Smail & Blundell 2013). However, theoretical models have also suggested that these haloes may instead be powered by cooling from gas in so-called ‘cold-flows’ (e.g. Fardal et al. 2001; Dekel et al. 2009). The spatially resolved dynamics and line profiles of these Ly $\alpha$  haloes, as well as their chemical enrichment, should be able to differentiate which mechanism is responsible for their formation (Bower et al. 2004; Smail & Blundell 2013).

The two-dimensional Ly $\alpha$  surface brightness distributions (e.g. Matsuda et al. 2012) or one-dimensional kinematics of high-redshift radio galaxies (e.g. van Ojik et al. 1997; Binette et al. 2000; Villar-Martín et al. 2003; Ohyama & Taniguchi 2004; Matsuda et al. 2006; Humphrey et al. 2007, 2009; Yang et al. 2011, 2014) suggest that the central AGN plays an important role in shaping the environments around massive, high-redshift galaxies on  $\gtrsim 10$ s of kpc scales. For example, observations have revealed that the spatial extent of the Ly $\alpha$  emitting gas is correlated with the spatial scales of the jets, whilst the distortion seen in the Ly $\alpha$  morphology is also typically correlated with the distortion in the radio emission (the extended emission line region morphology always appears to be brightest on the side of the radio lobes that is closer to the nucleus; McCarthy, van Breugel & Kapahi 1991; Tadhunter et al. 2000), suggesting that powerful radio sources are (at least partly) responsible for environmental effects on large scales. In terms of the large-scale environment, van Ojik et al. (1997) showed that the galaxies with radio jets that are extended on scales smaller than  $\lesssim 50$  kpc have the strongest strong H I absorption seen against Ly $\alpha$  (and likewise, those with radio extents  $\gtrsim 50$  kpc do not show strong absorbers). One explanation is that when radio sources grow they destroy the H I. However, this model also requires a duty cycle in which the ‘feedback’ expels gas, which cools then to form a shell of H I. A subsequent ‘feedback’ event then ionizes the gas. This model may also explain why the dynamics of the gas in the inner halo (located within the radio source) tend to be turbulent ( $\sigma \sim 700\text{--}1500$  km s $^{-1}$ ) whilst the out halo is more quiescent ( $\sigma \sim 300$  km s $^{-1}$ ; van Ojik et al. 1996).

To measure the energetics of the Ly $\alpha$  emission, search for and place dynamical constraints on the outflowing material requires resolved spectroscopy. However, relatively few galaxies have been studied using their two-dimensional Ly $\alpha$  velocity field, as required to truly understand their origin. The first attempt to derive the morphologies and dynamics of extended Ly $\alpha$  haloes was made by Hippelein & Meisenheimer (1993) who found a coherent and spatially extended ( $\sim 100$  kpc $^2$ ) and moderate column,  $n(\text{H I}) \sim$

$10^{15}$  cm $^{-2}$ , H I absorber in front of a 4C radio galaxy at  $z = 3.8$  (see also Adam et al. 1997). However, relatively few galaxies have been studied using their two-dimensional Ly $\alpha$  velocity field, as required to truly understand their origin (e.g. see Bower et al. 2004; Wilman et al. 2005; Villar-Martín et al. 2007b; Sánchez & Humphrey 2009; Weijmans et al. 2010; Martin et al. 2014, for a few examples). In part, this is due to the high redshift and hence large luminosity distances required to redshift Ly $\alpha$  into the optical band, which means that spatially resolving the low surface brightness features in the outer halo have, until now, been beyond the sensitivity limits of most instruments (even on 8-m telescopes). However, with the commissioning of the sensitive Multi Unit Spectroscopic Explorer (MUSE) on the European Southern Observatory (ESO)/Very Large Telescope (VLT), it is now possible to carry out these observations and so determine the nature of extended Ly $\alpha$  haloes.

In this paper, we exploit MUSE observations to determine the nature of extended Ly $\alpha$  halo around a powerful radio galaxy, TN J1338–1942 at  $z = 4.1$  (hereafter TN J1338). TN J1338 was identified as hosting a giant Ly $\alpha$  halo by Venemans et al. (2002). In a subsequent paper, Venemans et al. (2007) (see also Miley et al. 2004) identified 20 Ly $\alpha$  emitters within a projected distance of 1.3 Mpc and 600 km s $^{-1}$  of the radio galaxy (an overdensity of 4–15 compared to the average field at this redshift), suggesting a mass for the structure of  $M \sim 5 \times 10^{14} M_{\odot}$  which makes structure a likely ancestor of a massive galaxy cluster at the present day (with the radio galaxy likely to be a brightest cluster galaxy in formation). This high-redshift radio galaxy remains one of the brightest and most luminous known in Ly $\alpha$  ( $L_{\text{Ly}\alpha} \sim 5 \times 10^{44}$  erg s $^{-1}$ ). Both its Ly $\alpha$  profile and radio structure are very asymmetric (De Breuck et al. 1999; Wilman et al. 2004), which indicates strong interaction with dense gas, and the rest-frame radio luminosity is comparable to that of the most luminous 3C radio sources ( $P_{178\text{ MHz}} \sim 4 \times 10^{35}$  erg s $^{-1}$  Hz $^{-1}$  sr $^{-1}$ ). The MUSE observations presented here allow us to map the emission within the  $\sim 150$  kpc long Ly $\alpha$  halo, matching the sensitivity of previous narrow-band Ly $\alpha$  imaging of this structure, but with the *crucial* advantage of high spectral resolution kinematics, necessary to differentiate the signatures of infall or outflow (Bower et al. 2004; Wilman et al. 2005; Adams, Hill & MacQueen 2009).

The structure of this paper is as follows. In Section 2 we present the MUSE observations and data reduction. In Section 3 we discuss the morphology and energetics of the Ly $\alpha$  halo and those of the H I absorbers seen against the underlying emission. In Section 4 we present our conclusions. Throughout this paper, we adopt a cosmology with  $\Omega_{\text{m}} = 0.27$ ,  $\Omega_{\Lambda} = 0.73$  and  $H_0 = 71$  km s $^{-1}$  Mpc $^{-1}$  giving an angular scale of 7.0 kpc arcsec $^{-1}$  at  $z = 4.1$ .

## 2 OBSERVATIONS AND DATA REDUCTION

We observed TN J1338 with MUSE for a total of 9.0 h between 2014 April 30 and 2014 June 30 during a combination of commission and Science Verification time. The MUSE integral field unit (IFU) provides full spectral coverage spanning 4770–9300 Å, a contiguous field of view of  $60 \times 60$  arcsec $^2$ , with a spatial sampling of 0.2 arcsec pixel $^{-1}$  and a spectral resolution of  $R = 3000$  at  $\lambda = 6200$  Å (the wavelength of the Ly $\alpha$  at  $z = 4.1$ ). The observations were carried out in dark time, good sky transparency and 0.7 arcsec V-band seeing. Each 1 h observation was split into 1800 s exposures with a small (2 arcsec) dither. We obtained two overlapping pointings; the first centred at  $\alpha: 13:38:28.0$ ,  $\delta: -19:42:24$  and a second, offset by approximately 30 arcsec at  $\alpha: 13:38:25.0$ ,  $\delta: -19:42:32$ . Both

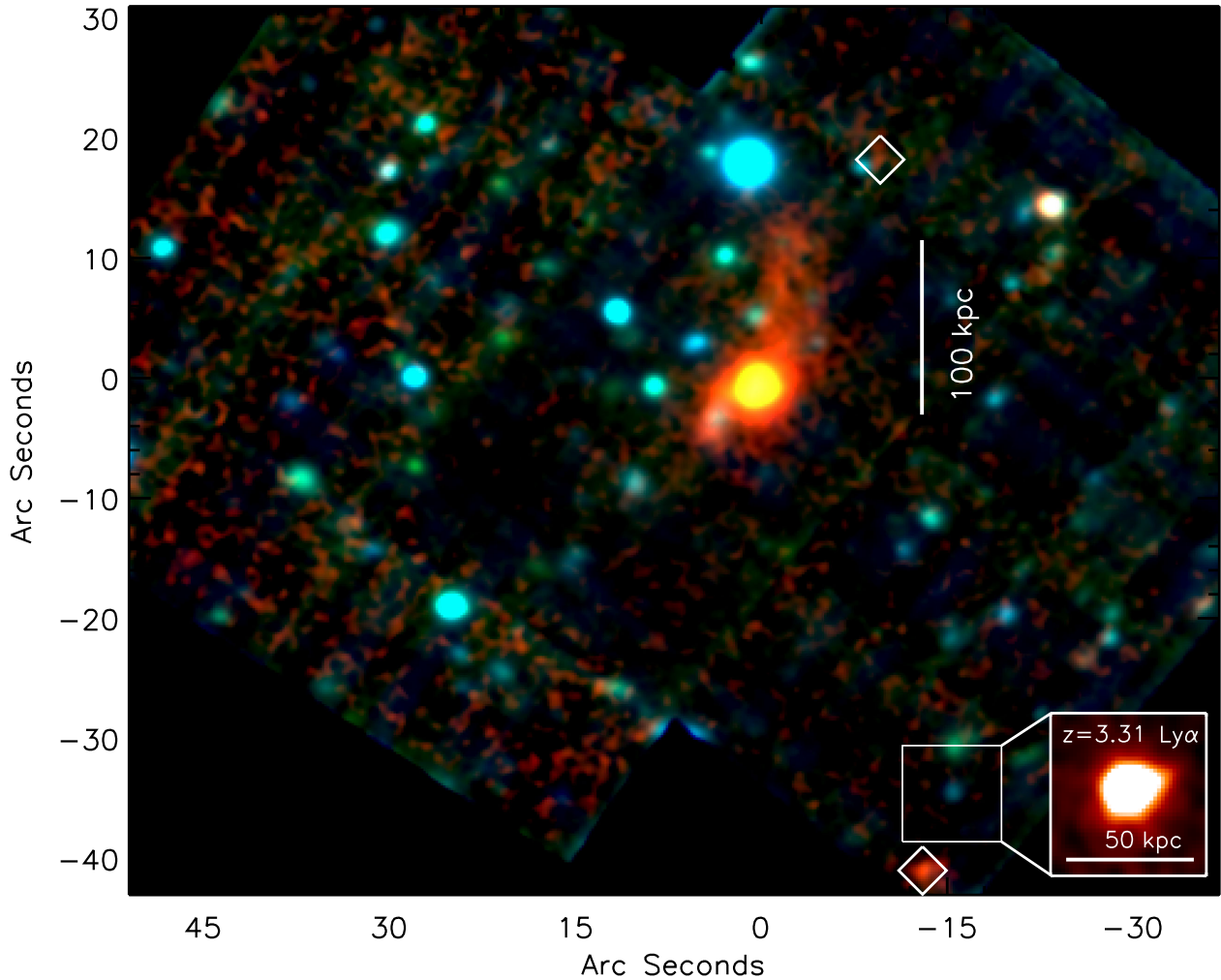


**Figure 1.** Colour ( $V, I, \text{Ly}\alpha_{z=4.1}$ ) image of the field around TN J1338 from the MUSE observations. This colour image illustrates the full extent the giant halo around the  $z = 4.1$  radio galaxy. Moreover, a search for other emission lines within the MUSE cube identifies a new giant ( $\sim 60$  kpc) halo around a foreground  $z = 3.31$  galaxy located to the south-west of the radio source. We also mark the positions of the two  $z = 4.1$  galaxies in the halo of the radio galaxy (open diamonds). The origin of the image is centred on the radio galaxy at  $\alpha: 13:38:26.1, \delta: -19:42:30.5$  (J2000).

pointings cover the  $z = 4.1$  radio galaxy and the final field of view is  $1.5 \times 1.0$  arcmin<sup>2</sup> (Fig. 1).

To reduce the data, we use the MUSE pipeline through ESOREX which wavelength calibrates, flat-fields the spectra and forms the data cube (Weilbacher et al. 2014). Because of the excellent flat-field stability of MUSE, sky subtraction was performed on each individual cube by identifying and subtracting the sky emission using blank areas of sky at each wavelength slice (i.e. no additional sky-only observations are required), and the final mosaic was then constructed using an average with a  $3\sigma$  clip to reject cosmic rays after registering the stars in continuum images from each individual cube.

A visual inspection of the final data cube reveals a very strong detection of the extended Ly $\alpha$  emission from the  $z = 4.1$  halo at 6200 Å as well as Ly $\alpha$  emission from a number of galaxies at the same redshift. In Fig. 1 we show a colour image of the field generated from the MUSE cube. In this image, we use the continuum from the wavelength ranges 4900–6900 and 6900–9000 Å as the blue and green images, respectively, whilst the red image is generated by collapsing the cube over the wavelength range 6100–6200 Å (which covers the Ly $\alpha$  from the  $z = 4.1$  radio galaxy). The strong,

extended Ly $\alpha$  emission can clearly be seen, with a spatial extent of  $\sim 150 \times 80$  kpc<sup>2</sup>.

We note that a search for line emitters within the cube also detects a second strong, spatially extended Ly $\alpha$  halo around a red  $z = 3.31$  galaxy located approximately  $\sim 30$  arcsec to the south-west of TN J1338 (Fig. 1) which appears to lie in an overdensity comprising a number of other star-forming galaxies and AGN at this redshift. In addition, a large number of foreground [O II], [O III] and Ly $\alpha$  emitters are detected in this volume. These will be discussed in a subsequent paper (Urrutia et al., in preparation).

### 3 ANALYSIS AND DISCUSSION

#### 3.1 Morphology and energetics of the Ly $\alpha$ halo

The morphology of the Ly $\alpha$  emission (Fig. 1) is very similar to that seen in the FORS 2 narrow-band imaging from Venemans et al. (2007), which has similar surface brightness limits as the Ly $\alpha$  narrow-band image created from the MUSE cube (collapsing the cube over 120 Å around the Ly $\alpha$  yields an image with a  $5\sigma$  line flux detection in a 1.2-arcsec aperture of  $f_{5\sigma} = \sim 8 \times 10^{-18}$  erg s<sup>-1</sup> cm<sup>-2</sup>

which is similar to that of the narrow-band image from Venemans et al. 2007;  $f_{5\sigma} = 6 \times 10^{-18} \text{ erg s}^{-1} \text{ cm}^{-2}$ ). Indeed, the morphology of the source shows a strong, spatially extended core which has a diameter of approximately 5 arcsec with a lower surface brightness halo which is extended along a roughly north–south direction which extends over a  $\sim 20$  arcsec (150 kpc) in extent. The elongated Ly $\alpha$  morphology is also consistent with the direction of the radio jets (Fig. 1), although the strongest jet emission is contained within the central  $\sim 10$  kpc, which may be indicative of previous AGN activity (which ionized the extended halo and which is now seen in Ly $\alpha$  emission as the gas cools). We note that the elongated morphology of the Ly $\alpha$  – in the same direction as the radio emission – is consistent with that seen in a number of other high-redshift radio galaxies (Röttgering & Pentericci 1999).

As an order-of-magnitude estimate of the total H II mass responsible for the Ly $\alpha$  emitting halo, we can assume case B recombination and that the gas is at a temperature of  $10^4$  K, and following De Breuck et al. (1999), using the total Ly $\alpha$  emission intensity (corrected for absorption, see Section 3.3), the total H II mass is approximately  $M(\text{H II}) \sim 10^9 (f_5 L_{44} V_{70})^{0.5} M_{\odot}$ , where  $f_5$  is the volume filling factor of  $10^{-5}$  (McCarthy et al. 1990),  $L_{44}$  is the Ly $\alpha$  luminosity in units of  $10^{44} \text{ erg s}^{-1}$  and  $V_{70}$  is the volume of the region in units of  $10^{70} \text{ cm}^3$ . Adopting a size of  $150 \times 80 \times 80 \text{ kpc}^3$  we derive  $M(\text{H II}) \sim 4 \times 10^9 M_{\odot}$ .

The spatial extent of the Ly $\alpha$  halo in TN J1338 is comparable to that seen in a number of other high-redshift radio galaxies (van Ojik et al. 1997; Humphrey et al. 2007). Indeed, extended Ly $\alpha$  haloes are common around high-redshift radio galaxies, extending up to  $\sim 250$  kpc – far beyond the continuum structures revealed by *Hubble Space Telescope* (*HST*) images (e.g. Villar-Martín et al. 2003). Moreover, the spatial extent of the Ly $\alpha$  emitting halo around high-redshift radio galaxies also appear to correlate with the size of the radio emission (van Ojik et al. 1997) (although of course, this is likely to be a selection effect since the larger haloes are likely to be more easily detectable around powerful active galaxies since the active nucleus provides a more intense supply of ionizing photons). Blind narrow-band surveys have also identified giant Ly $\alpha$  emitting haloes around star-forming galaxies with (relatively) low-luminosity AGN (Matsuda et al. 2011) as well as in structures containing multiple radio-quiet quasars (e.g. Cantalupo et al. 2014), suggesting that while an AGN may play an important role in providing the ionizing source of radiation to ionize the halo, it is not a requirement. Indeed, the Ly $\alpha$  blobs (LABs) also have spatial extents up to 180 kpc and the Ly $\alpha$  emission can be attributed to either photoionization from the AGN or star formation from the host galaxies (Geach et al. 2009).

What powers the Ly $\alpha$  emission in the extended halo of TN J1338 is unclear. As Fig. 1 shows, the Ly $\alpha$  halo extends over  $\sim 10 \times$  that of the radio jets detectable at GHz radio frequencies, which are contained within the central  $\sim 10$  kpc. One possible interpretation is that the emission in the extended halo is powered by the cooling of pristine gas within a dark matter halo (Fardal et al. 2001; Nilsson et al. 2006). However, the far-infrared luminosity of TN J1338 implied from *Herschell*/Spectral and Photometric Imaging Receiver (SPIRE) and James Clerk Maxwell Telescope (JCMT)/Submillimetre Common-User Bolometer Array (SCUBA) 850  $\mu\text{m}$  observations is  $L_{\text{IR}} = 7 \pm 1 \times 10^{12} L_{\odot}$  (SFR = 700  $M_{\odot} \text{ yr}^{-1}$ ; Drouart et al. 2014) which gives a ratio of total Ly $\alpha$ /IR luminosity of  $\sim 1 \times 10^{45}/4 \times 10^{46} = 0.03$ . This luminosity ratio is similar to that from the AGN luminosity ( $L_{\text{AGN}} \sim 2 \times 10^{46} \text{ erg s}^{-1}$ ; Drouart et al. 2014) which gives  $L_{\text{Ly}\alpha}/L_{\text{AGN}} = 0.05$ . Thus, only a small fraction of either the in-

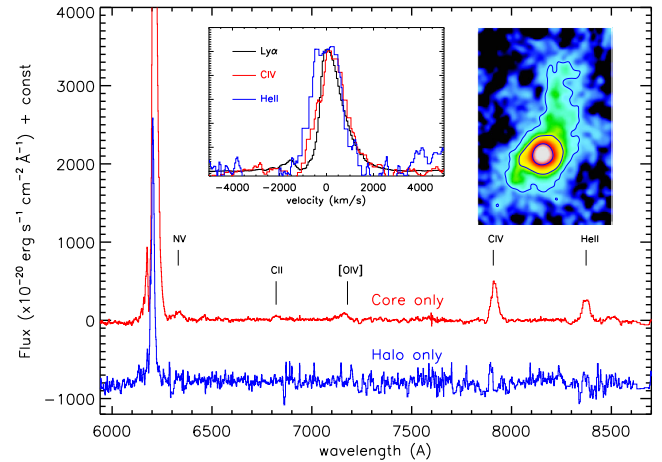


**Figure 2.** The spectrum extracted from the core of the Ly $\alpha$  halo compared to that of the extended halo. The core spectrum shows strong emission lines associated with the AGN activity (e.g. N v, [O IV], C IV and He II). The emission from the halo (which should exclude any seeing-related contamination from the core, but will not exclude scattered emission within the halo) also shows weak C IV emission. The Ly $\alpha$  image of the halo (inset) shows the two regions from which the core and halo were extracted (for the core, all pixels within the inner contour were included and for the halo, all pixels between the second and third contours were included). The second inset compares the line profile of the Ly $\alpha$ , C IV and He II from the core region. In this panel, we use the He II emission to define the systemic redshift,  $z = 4.1057$  (and transform the Ly $\alpha$ , C IV and He II to the same rest-frame velocity scale). In the core region, the Ly $\alpha$  and C IV share the same characteristic (asymmetric) line profile, implying the presence of C IV in the absorbing material and suggesting that any absorbing materials must be enriched in metals.

frared (star formation) or AGN luminosity is required to power the Ly $\alpha$  emission. However, we note that the high Ly $\alpha$ /He II ratio averaged over the halo is  $\text{Ly}\alpha/\text{He II } \lambda 1640 = 18.7 \pm 0.5$  (see Section 3.2) which is difficult to explain with AGN photoionization only (Villar-Martín et al. 2007a), and suggests we are likely to be observing a combination of energy sources that are heating the halo.

### 3.2 Spatially resolved structure

Before determining the velocity structure of the halo, we first define the systemic redshift of the galaxy by extracting a spectrum from a  $1 \times 1 \text{ arcsec}^2$  region centred on the UV (and radio) continuum counterpart. Unfortunately, no strong photospheric absorption features are present, but there are strong detections of Ly $\alpha$ , C IV  $\lambda 1549$  and He II  $\lambda 1640$  (see Fig. 2). Since the Ly $\alpha$  and C IV are resonant lines, we use the He II emission line and fit a single Gaussian profile, deriving a redshift of  $z = 4.1057 \pm 0.0004$  and a full width at half-maximum (FWHM) of  $35 \pm 3 \text{ \AA}$  (or  $1250 \pm 100 \text{ km s}^{-1}$ ). In all following sections, we adopt  $z = 4.1057$  as the systemic redshift when comparing velocities or velocity differences.

To investigate the spectral properties of the core and halo, we begin by extracting two spectra, one from a circular  $\sim 3 \times 3 \text{ arcsec}^2$  region centred on the continuum counterpart (the core of the galaxy), and a second from the extended halo (excluding the core region), and we show these two spectra in Fig. 2. The core spectrum shows strong emission lines associated with the AGN (e.g. N v, [O IV], C IV and He II). The emission from the halo (which should exclude any seeing-related contamination from the core, but will not exclude scattered emission within the halo) also shows weak C IV emission. The detection of heavy elements (in particular C IV) in the extended

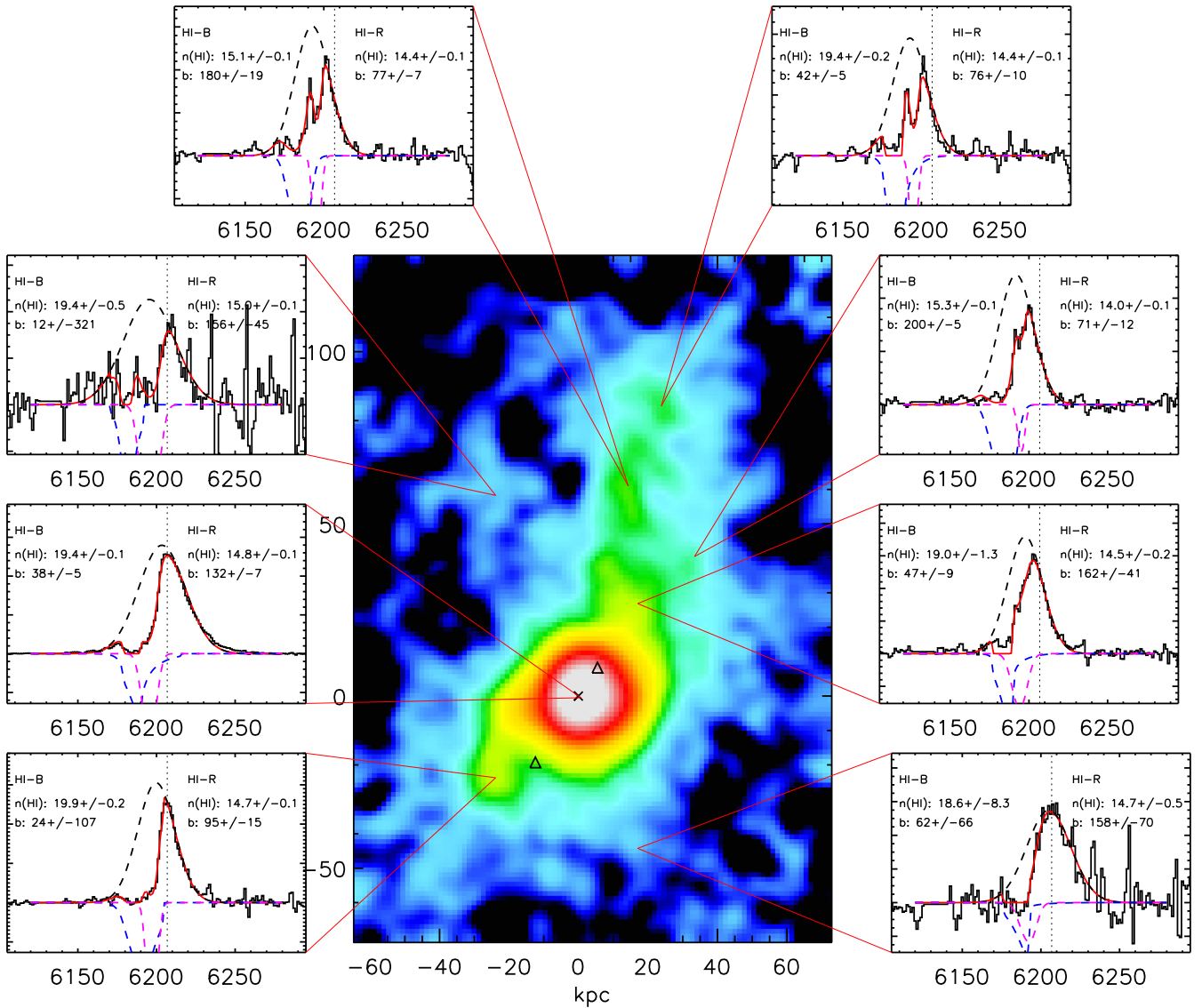


**Figure 3.** Upper panel: continuum subtracted, wavelength collapsed, narrow-band image of the TN J1338 Ly $\alpha$  halo from the MUSE cube (collapsed over the wavelength range 6100–6300 Å). The cross denotes the position of the UV continuum (and radio) counterparts, and the open triangles show the positions of the radio hotspots (end points of the jets) from De Breuck et al. (1999) indicating the compact size of the radio source compared to the highly extended Ly $\alpha$  halo. We also show example spectra of regions within the halo. These are typically extracted from  $2 \times 2$  arcsec $^2$  regions, and in all cases, the line profile is best fit by two H I absorbers superimposed on an underlying Gaussian emission profile. Both absorbers have a covering factor of unity; the first absorber, H I-B, appears blueshifted from the (underlying) Gaussian emission line profile by  $\sim -700$  km s $^{-1}$  and has a column density of  $n(\text{H I}) \sim 10^{19.3}$  cm $^{-2}$  whilst the second absorber, H I-R, is much closer to the underlying halo emission,  $\Delta v \sim -200$  km s $^{-1}$  but has a much lower column density,  $n(\text{H I}) \sim 10^{14.5}$  cm $^{-2}$ .

halo suggests that the halo is already metal enriched (see also Villar-Martín et al. 2003; Binette et al. 2006).

The line ratios from carbon, nitrogen or helium compared to hydrogen can be used to infer the physical conditions within the diffuse halo. Although the C IV and He II emission lines lie in regions of high atmospheric OH emission, we derive line ratios (or limits) of  $[\text{C IV}]/\text{Ly}\alpha = 0.082 \pm 0.003$  and  $0.064 \pm 0.013$  for the ‘core’ and ‘halo’, respectively. For the He II/Ly $\alpha$  ratio, we derive  $\text{He II}/\text{Ly}\alpha = 0.044 \pm 0.003$  and  $<0.075$  for the ‘core’ and ‘halo’, respectively – consistent with stellar or power-law photoionization models with metallicities ranging from 0.05 to 1  $Z/Z_{\odot}$  (Binette et al. 2006; Villar-Martín et al. 2007a).

Next we extract a number of spectra across the halo by integrating  $\sim 2 \times 2$  arcsec $^2$  regions and show these in Fig. 3. Whilst the strong

Ly $\alpha$  emission is clearly evident, it is also apparent that the emission line is asymmetric. One possible interpretation of the Ly $\alpha$  emission line profile is that it naturally arises from the transfer of Ly $\alpha$  radiation through a neutral screen. If the Ly $\alpha$  photons have to travel through a region of neutral hydrogen, they will resonantly scatter until they Doppler shift into the wings where the opacity is lower. Such a phenomenon will give rise to either a double-peaked profile (Adams 1975; Dijkstra, Haiman & Spaans 2006) or, depending on the geometry and kinematics of the neutral gas, an asymmetric profile in which one of the peaks is stronger. However, for this to be a viable explanation of the observed line profile in TN J1338, we require the Ly $\alpha$  to be embedded in a (partial) cocoon of neutral hydrogen of large optical depth. On the other hand, the asymmetry of the emission line, and the sharpness of the deep trough(s) suggest

that H I absorption is far more probable (e.g. Rottgering et al. 1995; van Ojik et al. 1997; Wilman et al. 2004).

Within the central regions of the halo, the asymmetric Ly $\alpha$  profile was first studied using high-resolution Ultraviolet and Visual Echelle Spectrograph (UVES) by Wilman et al. (2004) who showed that the line emission is best fit with an underlying Gaussian profile with two H I absorbers with column densities  $n(\text{H I}) \sim 10^{15.0}$  and  $\sim 10^{19.7} \text{ cm}^{-2}$  for H I-B and H I-R, respectively. As we shall see, a similar combination of absorbers is required to reproduce our spectra across all of the halo.

To describe the line profile, we begin by fitting a Gaussian profile emission line with a H I absorber (which is described by a Voigt profile). However, in all of the regions shown in Fig. 3, this fit fails to provide an adequate description of the line, and instead two H I absorbers are required to adequately describe the line profile (see also Wilman et al. 2004). The first of these absorbers, which we label H I-R (the most redshifted) is typically offset from the central (underlying) Gaussian profile by  $\sim -270 \text{ km s}^{-1}$ , has a column density of  $n(\text{H I}) \sim 10^{14.5} \text{ cm}^{-2}$  and Doppler parameter of  $b = 100 \pm 4 \text{ km s}^{-1}$  whilst the second absorber H I-B (the most blueshifted) is typically offset from the underlying Gaussian profile by  $\sim -1200 \text{ km s}^{-1}$  but with a much higher column density,  $n(\text{H I}) \sim 10^{19.3} \text{ cm}^{-2}$  and  $b = 170 \pm 5 \text{ km s}^{-1}$ . Within the halo, the underlying Gaussian profile has an average velocity dispersion of  $\sigma = 570 \pm 13 \text{ km s}^{-1}$ , in agreement with the velocity dispersions of the He II emission line, and much broader than the two absorbers. The velocity dispersion of the underlying emission is peaked at the position of the radio galaxy (and the radio jets), with  $\sigma = 750 \pm 20 \text{ km s}^{-1}$ . This may reflect two components of the halo: the inner halo where there is a strong interaction between the radio plasma and the gas, and the outer (more quiescent) halo, located outside the radio source (van Ojik et al. 1996). In contrast, the much smaller velocity dispersion of the absorbing gas is more readily explained if these absorbers lie at relatively large distances from the parent galaxy. We will discuss the spatially resolved properties of these absorbers in Section 3.3.

Finally, we note that van Ojik et al. (1997) showed that most high-redshift radio sources with radio jets within  $\sim 50 \text{ kpc}$  of the central galaxies show strong H I absorption against their Ly $\alpha$  emission. This may suggest that when the radio sources grow, they destroy the H I. Since the radio emission in TN J1338 is located within  $\sim 10 \text{ kpc}$  of the galaxy, this radio source clearly falls into first category. Within this scenario, there must be a duty cycle with the feedback expelling Ly $\alpha$  emitting gas, which cools to form a shell of H I around it, and a subsequent feedback event ionizes the gas.

### 3.3 Dynamics of the H I absorbers

As can be seen from Fig. 3, one of the striking results from our MUSE observations is the coherence and spatial extent of both absorbers. The most blueshifted absorber, H I-B, which has  $n(\text{H I}) \sim 10^{19.3} \text{ cm}^{-2}$  appears to be spatially extended across the entire  $150 \times 80 \text{ kpc}^2$  structure. The second absorber, H I-R, which has a significantly lower column density  $n(\text{H I}) \sim 10^{14.5} \text{ cm}^{-2}$  also appears to be extended over the same area. Thus, the covering factor of both absorbers appears to be close to unity. Evidence for extended reservoirs of neutral gas has been seen in a number of giant Ly $\alpha$  haloes around high-redshift radio galaxies (van Ojik et al. 1997; Binette et al. 2000; Villar-Martín et al. 2003; Wilman et al. 2004) as well as star-forming galaxies (Bower et al. 2004; Wilman et al. 2005; Weijmans et al. 2010).

To examine whether the H I absorbers are ‘pristine’ – as suggested by the cold-flow model – in Fig. 2 we compare the Ly $\alpha$ , C IV and He II emission line profiles (transformed to the same rest-frame velocity scale). Although the C IV emission has lower signal-to-noise ratio (S/N), it is clear that the Ly $\alpha$  and C IV share the same characteristic (asymmetric) line profile, implying the presence of C IV in the absorbing material (without other species, it is difficult to derive the ionization of the absorbing material, but it appears that this absorbing gas must be metal enriched, arguing against a model in which the Ly $\alpha$  results from the cooling of pristine material).

With the two-dimensional data provided by MUSE, next, we construct a spatially resolved map of the dynamics and column density across the halo. To achieve this, at each spatial pixel, we average the surrounding  $1 \times 1 \text{ arcsec}^2$  region, and measure the S/N. If the S/N > 50, we then attempt to fit the emission line profile with an underlying Gaussian profile with two H I absorbers, allowing the centroid, intensity and line-width (FWHM in the case of the Gaussian profile and Doppler  $b$ -parameter in the Voigt profile) to be free parameters. If the S/N is not sufficiently high to allow a fit, we adaptively bin up to  $3 \times 3 \text{ arcsec}^2$  (in steps of 0.2 arcsec) and refit.

In Fig. 4 we show the velocity field of the underlying Gaussian emission, as well as that of the two H I absorbers. The underlying emission has a strong velocity gradient ( $\sim 700 \text{ km s}^{-1}$ ) across the  $150 \text{ kpc}$  in projection. At the position of the galaxy, the Ly $\alpha$  is blueshifted by  $\sim 150 \text{ km s}^{-1}$  from the systemic, and this velocity offset decreases up to  $\sim 1200 \text{ km s}^{-1}$  towards to north-west. The H I absorber which has a velocity closest to the underlying emission, H I-R, does not have a strong velocity gradient across the major axis. However, the most blueshifted absorber, H I-B, is blueshifted from the underlying emission by  $\sim 700 \text{ km s}^{-1}$  with a velocity field that apparently mirrors that of the underlying Gaussian profile. To highlight these differences, we extract the dynamics through a pseudo-slit from the major kinematic axis of the halo and show this in Fig. 5.

Turning to the column density maps, Fig. 4 shows that both of the H I columns are remarkably uniform (although at two distinct velocities), with both remaining as single systems of the full extent of the Ly $\alpha$  emission. The spatial and kinematic coherence of the absorbers suggest they may be physically distinct from the background source. Using the column densities and sizes, the total neutral mass of H I-B and H I-R are  $M_{\text{H I-B}} \sim 10^9 M_{\odot}$  and  $M_{\text{H I-R}} \sim 10^5 M_{\odot}$ . The total hydrogen mass of the absorber depends on the ionization state. Photoionization models of absorption systems with column densities in the range  $n(\text{H I}) = 10^{19-20} \text{ cm}^{-2}$  suggest average intergalactic medium (IGM) neutral fractions at  $z = 4$  of  $X_{\text{H I}} \sim 1.5\text{--}10$  (McQuinn, Oh & Faucher-Giguère 2011). Of course, these values may represent upper limits in an overdense region which self-shields from UV radiation. Nevertheless, this suggests a total mass for the most massive absorber, H I-B, of  $\sim 10^{10} M_{\odot}$ .

#### 3.3.1 Inflow or outflow?

Previous observations of high-redshift radio galaxies have identified very strong (high column density) absorbers seen against the Ly $\alpha$  profiles (Hippelein & Meisenheimer 1993; van Ojik et al. 1997; Humphrey et al. 2007). The interpretation of this absorption is the fortuitous alignment with the intervening Ly $\alpha$  forest absorption, which may be enhanced in the biased regions around massive, high-redshift galaxies. Whilst the properties of absorbing haloes around radio galaxies have been studied in detail, most studies have been

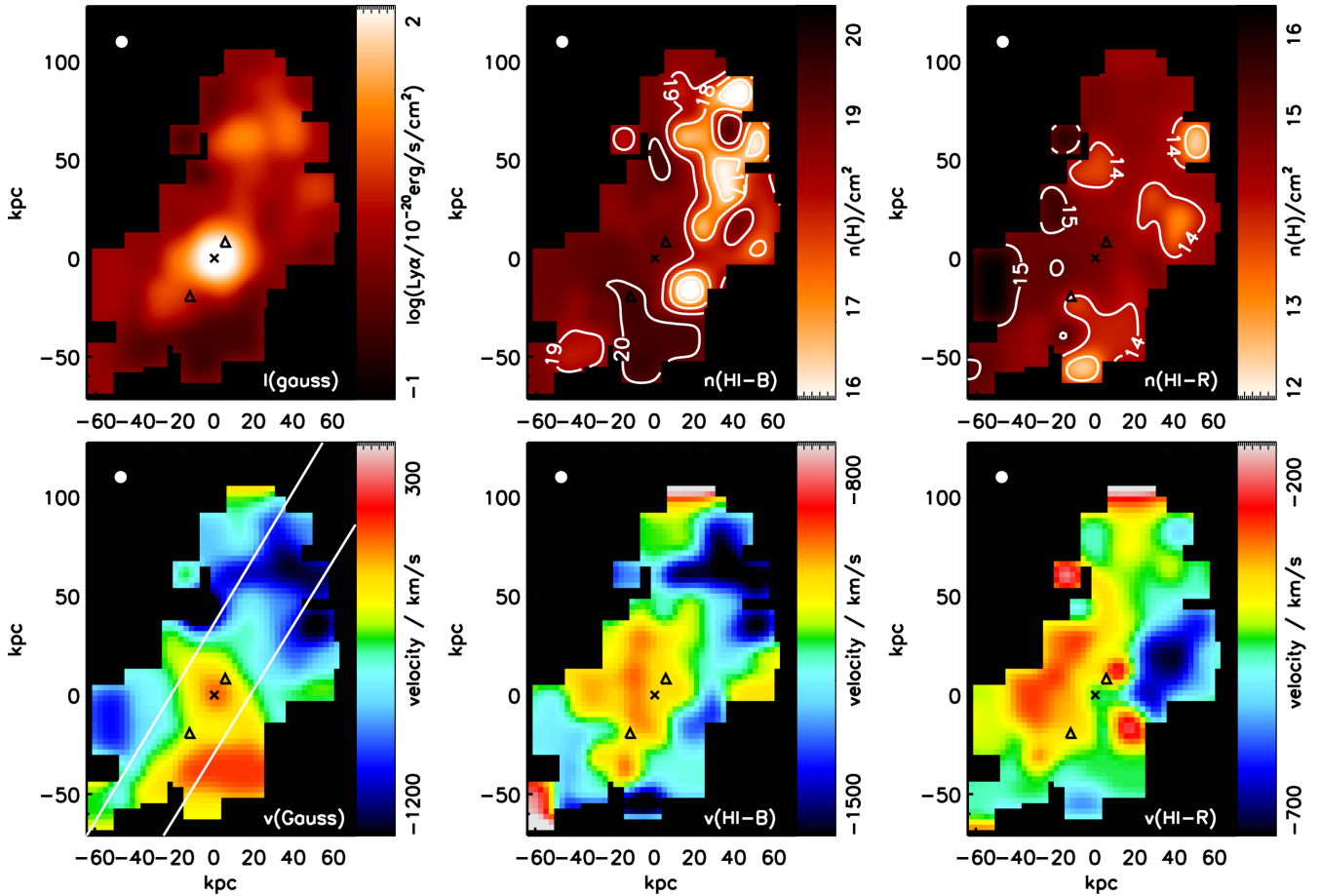


**Figure 4.** Top row: intensity map of the underlying Ly $\alpha$  Gaussian emission line profile (left), and spatial column density distribution of H I-B (middle) and H I-R (right). Bottom row: velocity structure of the Gaussian profile, H I-B and H I-R. In all cases, the velocity scale is set by the systemic, as measured from the He II emission:  $z = 4.1057$ . The solid point in the top left-hand corner of each panel denotes the 0.7 arcsec FWHM seeing disc. In each panel, we also show the position of the radio core (and continuum counterpart of the galaxy; cross) and the radio lobes (open triangle). The underlying Gaussian emission line profile shows a maximum velocity gradient of  $\sim 1000$  km s $^{-1}$  across the 150 kpc (in projection). At the position of the galaxy, the Ly $\alpha$  is blueshifted by  $\sim 150$  km s $^{-1}$  from the systemic. The velocity dispersion profile of the underlying emission (which has an average value of  $\sigma = 570 \pm 13$  km s $^{-1}$ ) is peaked at the position of the radio galaxy and the radio jets, which may reflect the interaction of the radio plasma and the gas. Both H I-B and H I-R have covering factors of unity. H I-B appears blueshifted from the (underlying) Gaussian emission line profile by  $\sim -700$  km s $^{-1}$  and has an average column density of  $n(\text{H}) \sim 10^{19.3}$  cm $^{-2}$ . This material is most likely associated with an outflowing shell of material, and we estimate the mass in the shell must be of order  $\sim 10^{10} M_{\odot}$ . The second absorber H I-R is much closer to the underlying halo emission in velocity space,  $\Delta v \sim -200$  km s $^{-1}$  but has a much lower column density, with an average of  $n(\text{H}) \sim 10^{14.5}$  cm $^{-2}$ . This material is most likely to be associated with the low-density ICM between the outflowing shell and the Ly $\alpha$  halo.

limited to (either) low-resolution spectra and/or integrated spectra, but where it has been possible to spatially resolve the absorption, the implied covering factor is close to unity – on scales from 10 to 50 kpc – and the inferred mass of the neutral phase is  $\sim 10^7$ – $10^8 M_{\odot}$ . The absorbers also appear to be ubiquitous when seen against radio quiet galaxies, such as the giant LABs at  $z = 3.1$  which have also been studied in detail (Matsuda et al. 2011) (we note that the other absorber in this field also shows a strong, spatially extended absorber in the MUSE data; Urrutia et al., in preparation). For example, Matsuda et al. (2006) find that the fraction of LABs with absorbers seen against the Ly $\alpha$  emission are 83 per cent. However, the nature of the absorbing gas remains poorly understood even when two-dimensional spectra are available. In particular, two-dimensional spectra are required to test whether the neutral gas is likely to be in-falling or outflowing. With sufficient S/N and spectral (and spatial) resolution the spatially resolved dynamics of the neutral gas provided by MUSE, and its relation to the (underlying) emission

should allow us to distinguish between infall and outflow, and we consider both possibilities here.

In a scenario in which the absorber(s) around TN J1338 arise due to foreground material, the giant Ly $\alpha$  halo only provides the background (illuminating) screen from which the absorbers are decoupled. In this case, the coherence of absorbers may suggest we are seeing a sheet (or filament) with a projected separations from the radio galaxy of  $\sim 4$  and  $< 1$  Mpc (assuming a Hubble constant at  $z = 4.1$  of  $H(z) = 423$  km s $^{-1}$  Mpc). The low column density absorber, H I-R, is presumably within the virial radius of the halo associated with the radio galaxy since the velocity offset places it within  $\sim 1$  Mpc of the galaxy.

Whilst this interpretation is appealing since high-density IGM is expected to be seen around massive galaxies, there are a number of problems with this inflow model. First, the H I appears to be enriched, although this does not preclude them being unassociated with the radio galaxy, especially in an overdense (biased)

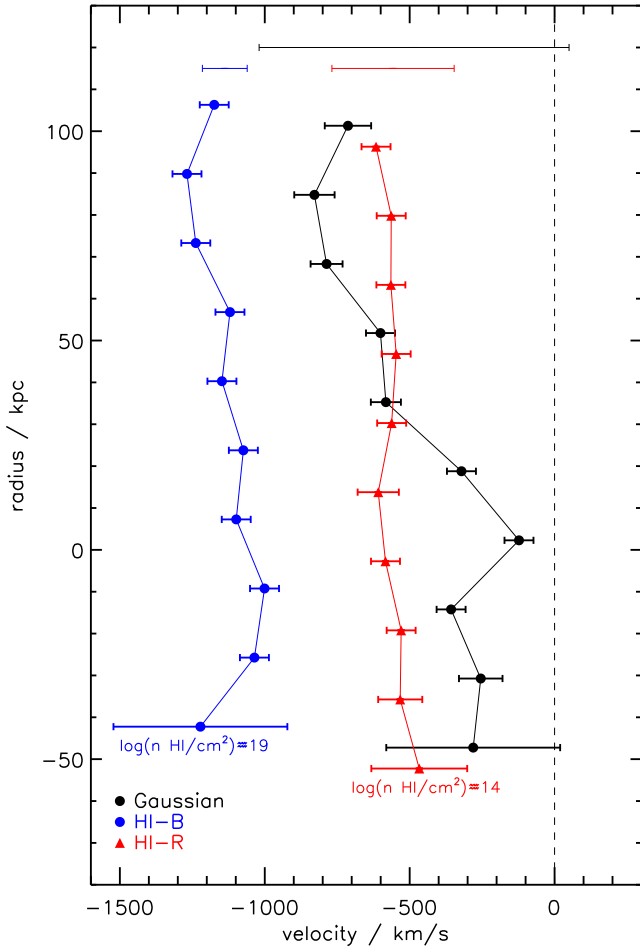


**Figure 5.** The velocity profile of the underlying Gaussian emission and the two absorbers extracted across the major axis of the Ly $\alpha$  halo (as shown in Fig. 4). The solid points and thick error bars denote the central velocity and the error on the central velocity, whilst the thinner errors at the top of the panel show the average width of the Gaussian ( $\sigma$ ) or Doppler  $b$ -parameter (absorbers) in each bin. The origin of the velocity and spatial axes is fixed on the radio galaxy, demonstrating that these motions do not reflect bulk rotation of gas around the radio galaxy if it lies at the bottom of the potential well (cf. van Ojik et al. 1997).

region. Second, the velocity structure of the underlying Ly $\alpha$  emission (which has an average velocity gradient across the halo of  $dv/dR \sim 4 \text{ km s}^{-1} \text{ kpc}^{-1}$ ) is mirrored by HI-B ( $dv/dR \sim 3 \text{ km s}^{-1} \text{ kpc}^{-1}$ ) strongly suggesting that the material associated with HI-B originated in the Ly $\alpha$  halo (which would then naturally explain the similarity in the Ly $\alpha$  and C IV line profiles). Third, across the halo, the low-density absorber, HI-R, has a median Doppler  $b$ -parameter of  $b = 170 \pm 3 \text{ km s}^{-1}$ . We can test if this is ‘typical’ of Ly $\alpha$  absorbers by using quasar sight lines. Fechner & Reimers (2007) and Schaye et al. (2000) derive column density and Doppler  $b$  parameters for neutral hydrogen in the Ly $\alpha$  forest at  $z = 2\text{--}4.5$ . In total, they detect  $\sim 1500$  absorbers with columns between  $\log n(\text{H I}/\text{cm}^{-2}) = 12\text{--}17$  and  $b = 5\text{--}200 \text{ km s}^{-1}$ . Cutting their sample to the same median column density as seen in HI-R,  $\log n(\text{H I}/\text{cm}^{-2}) = 14.5$ , the median Doppler parameter is  $b = 30 \pm 1 \text{ km s}^{-1}$ , a factor  $5.5 \pm 0.4$  lower (for the same median column density) as that seen in HI-R. Thus, it appears that the low column density absorber seen against the halo of TN J1338 does

not have the properties expected for simply being ‘average’ IGM, but instead has a much higher velocity width.

A more natural explanation for the absorbers is therefore that HI-B represents the outflowing material swept up in a wind shell ejected from the host galaxy and HI-R is the low-density material between this shell and the host. Galactic scale outflows from high-redshift galaxies, driven by the collective effects of star formation and supernovae winds (e.g. Pettini et al. 2002; Bower et al. 2004; Erb et al. 2006; Swinbank et al. 2007, 2009; Steidel et al. 2010; Martin et al. 2012; Newman et al. 2012) and/or AGN (e.g. Nesvadba et al. 2007; Alexander et al. 2010; Harrison et al. 2012, 2014; Martin et al. 2012; Genzel et al. 2014), have been studied for some time and outflow velocities reaching  $\sim 1000 \text{ km s}^{-1}$  in the ionized gas spread over 10s of kpc.

Can we explain the properties of the absorbers in such a model? Numerical models can be used to trace the evolution of the interstellar medium (ISM) following the energy injection into an ambient medium, thus making predictions for the effect of a starburst or AGN-driven wind on the ISM. For example, Krause (2005) use a hydro-dynamic code to model a galactic wind (due to star formation and supernova) on the ISM of a host galaxy and superimpose an AGN-driven jet. Assuming the wind starts long before the jet activity, the starburst first drives the wind in to a radiative bow shock, which then cools and is seen in Ly $\alpha$  absorption. When the jet reaches the shell, it may destroy it (at least partially) so that the larger sources are no longer absorbed (the shell eventually cools and fragments to form globular clusters). In this model, the power required to drive the wind is approximately  $L \gtrsim 5 \times 10^{43} \text{ erg s}^{-1} \sqrt{T/10^6 \text{ K}} (v_{\text{shell}} / 200 \text{ km s}^{-1})^4 (r_{\text{shell}}/25 \text{ kpc})$ . For the outflow in TN J1338, with  $v_{\text{shell}} \sim 1000 \text{ km s}^{-1}$  and  $r_{\text{shell}} \sim 200 \text{ kpc}$ ,  $L \sim 1 \times 10^{46} \text{ erg s}^{-1}$ . Although this calculation should be considered approximate, the luminosity required to drive the shell is consistent with the AGN luminosity of TN J1338,  $L_{\text{AGN}} \sim 2 \times 10^{46} \text{ erg s}^{-1}$  (Drouart et al. 2014).

Another approach is to consider the energy of the AGN (or star formation) and the likely time-scales involved. Assuming the outflow in TN J1338 is a coherent structure, the mass swept up in the shell must be of order  $M_{\text{outflow}} \sim 10^{10} M_{\odot}$  (for a neutral fraction of 10 per cent) and it will have a kinetic energy of  $\sim 10^{59} \text{ erg}$  (assuming a spherical shell with mass  $\sim 10^{10} M_{\odot}$  moving at  $1200 \text{ km s}^{-1}$  with respect to the galaxy). If the shell is located a minimum of  $\sim 200 \text{ kpc}$  from the radio galaxy (this minimum being set by the spatial extent of the Ly $\alpha$  halo and coherence of the absorber), then the *minimum* lifetime of the outflow is 100 Myr. Considering the AGN luminosity of this source,  $L_{\text{AGN}} \sim 2 \times 10^{46} \text{ erg s}^{-1}$  and a minimum time-scale of 100 Myr, the total energy available is  $\sim 5 \times 10^{61} \text{ erg}$ . Alternatively, considering star formation as the energy injection mechanism and assuming supernovae provide  $10^{49} \text{ erg } M_{\odot}^{-1}$  of stars formed, the energy provided by SNe will be  $\sim 10^{60} \text{ erg}$ . Thus energetically, this star formation or AGN could drive the wind if they are able to couple  $< 10$  per cent of their energy to the wind (and the energy in the wind should be considered a lower limit since the galaxy–shell distance is a lower limit).

We can also compare the mass in the absorber to the total ISM mass of the host galaxy. Fitting a modified blackbody to the *Herschel* 250–500  $\mu\text{m}$ , SCUBA 850  $\mu\text{m}$  and Max-Planck Millimeter Bolometer Array (MAMBO) 1.2 mm photometry of this galaxy (De Breuck et al. 2004; Drouart et al. 2014), adopting a dust emissivity of  $\beta = 1.5\text{--}2.0$  (Magnelli et al. 2012) and dust mass absorption coefficient of  $\kappa_{870 \mu\text{m}} = 0.15 \text{ m}^2 \text{ kg}^{-1}$  (Weingartner & Draine 2001), we estimate a cold dust mass of  $M_{\text{dust}} \sim 3 \times 10^8 M_{\odot}$ . For a dust-to-gas

ratio of  $\delta_{\text{DGR}} = 90$  (Bothwell et al. 2013; Swinbank et al. 2014), this suggests a  $\text{H}_2$  mass of  $M_{\text{H}_2} \sim 3 \times 10^{10} M_{\odot}$ , which is comparable to that estimated for other high-redshift radio galaxies (Miley & De Breuck 2008; Emonts et al. 2014). We caution that there is a factor of 3–4 $\times$  uncertainty on this value due to the (moderately low) S/N of the 850  $\mu\text{m}$  and 1.2 mm detections (and upper limits on the 250, 350 and 500  $\mu\text{m}$  photometry), the choice of dust model parameters and the uncertainty in the adopted dust-to-gas ratio. Nevertheless, the  $\text{H}_2$  mass of the ISM in the radio galaxy is similar to that estimated for the total mass of the two structures we see in absorption against the halo.

Will the gas escape the halo potential? If we consider a  $\sim 10^{11} M_{\odot}$  galaxy inside a dark halo with mass  $\sim 10^{13}$ – $10^{14}$  with NFW (Navarro, Frenk & White 1997) density profile, the gas would require a velocity greater than  $\sim 1000 \text{ km s}^{-1}$  to escape the halo (see also the calculation in Harrison et al. 2012). This is similar to the velocity seen in H I-B. However, some models have suggested that even massive outflows may stall in the galaxy halo (or in this case, the ‘group’ halo), and recollapse and cool at later times (along with new fuel supplies), resulting in re-ignition of star formation and further black hole growth (e.g. Lagos, Cora & Padilla 2008; Gabor et al. 2011; Hopkins et al. 2013), especially in group/cluster (or protocluster) environments (McCarthy et al. 2011).

In summary, while it is not possible to constrain definitively whether the AGN or star formation have driven the outflow, or the ultimate fate of outflowing gas, it appears that the H I absorbers are associated with activity occurring within the galaxy, and with outflow properties (high velocity, spatially extended and mass loaded) in broad agreement with the requirements of models that invoke AGN-driven outflows to regulate star formation and black hole growth in luminous AGN (Di Matteo et al. 2005; Hopkins & Elvis 2010; Debuhr et al. 2012). Even if the outflow does not escape the galaxy haloes, it may have sufficient energy to heat the halo and control the level of cooling in massive haloes at later times (e.g. Churazov et al. 2005; Gabor et al. 2011; McCarthy et al. 2011; Bower, Benson & Crain 2012).

## 4 CONCLUSIONS

We have used the MUSE integral field spectrograph to study the giant  $\text{Ly}\alpha$  halo around the high-redshift radio galaxy TN J1338 at  $z = 4.11$ . Our main observations reveal the following.

(i) Our observations map the intensity distribution and dynamics of the  $\text{Ly}\alpha$  halo which is extended over a region approximately  $150 \times 80 \text{ kpc}^2$ . In comparison, the radio jets are confined to the central  $\sim 10 \text{ kpc}$  of the halo, although the alignment of the extended  $\text{Ly}\alpha$  halo and radio jets may be indicative of previous AGN activity (which ionized the extended halo and which is now seen in  $\text{Ly}\alpha$  emission as the gas cools).

(ii) The spatial extent of the  $\text{Ly}\alpha$  halo in TN J1338 is one of the largest seen in high-redshift radio galaxies. We clearly detect the C IV emission in the extended halo suggesting that the gas in this extended halo is enriched.

(iii) Across the entire halo, the  $\text{Ly}\alpha$  emission line appears asymmetric. The line profile is best fit by two H I absorbers superimposed on an underlying Gaussian emission profile. One of the striking results from our MUSE observations is the coherence and spatial extent of both absorbers. Indeed, both absorbers have a covering factor of unity. The first absorber, H I-B, appears blueshifted from the (underlying) Gaussian emission line profile by  $\sim -700 \text{ km s}^{-1}$  and has a column density of  $n(\text{H I}) \sim 10^{19.3} \text{ cm}^{-2}$ . Since the velocity

structure of this absorber follows that of the underlying emission, this material is most likely associated with an outflowing shell of material, and we estimate the mass in the shell must be of order  $\sim 10^{10} M_{\odot}$ . By comparison to the AGN luminosity or star formation rate of the galaxy, we find that both could trivially drive the wind if they are able to couple  $\ll 0.1$  per cent of their energy to the wind. The second absorber, H I-R, is much closer to the underlying halo emission,  $\Delta v \sim -200 \text{ km s}^{-1}$  but has a much lower column density,  $n(\text{H I}) \sim 10^{14.5} \text{ cm}^{-2}$ . The Doppler  $b$ -parameter for this absorber is  $\sim 6\times$  higher than expected for the low-density IGM (at the same column density), suggesting that this is not just a typical intergalactic absorber, but instead that this material represents the low-density IGM between the outflowing shell and the  $\text{Ly}\alpha$  halo. We show that the energetics of the star formation or AGN could drive the outflow if it is able to couple a small fraction of the energy to the gas.

(iv) The underlying Gaussian emission line profile shows a velocity gradient of  $\sim 700 \text{ km s}^{-1}$  across the 150 kpc in projection. At the position of the galaxy, the  $\text{Ly}\alpha$  is blueshifted by  $\sim 150 \text{ km s}^{-1}$  from the systemic. The velocity dispersion profile of the underlying emission (which has an average value of  $\sigma = 570 \pm 13 \text{ km s}^{-1}$ ) is peaked at the position of the radio galaxy and the radio jets, which may reflect the interaction of the radio plasma and the gas.

(v) We identify two other  $z = 4.1$  emitters in the field of the radio galaxy which are presumably associated with the group/cluster within this overdensity. We also serendipitously identify a new giant  $\text{Ly}\alpha$  halo at  $z = 3.31$  approximately  $\sim 30 \text{ arcsec}$  to the south-west of TN J1338 which appears to be associated with a number of other star-forming galaxies and AGN at this redshift.

Finally, we can consider how the galaxy and outflow may evolve towards the present day. The outflowing shell will be both thermally and gravitationally unstable, and will eventually fragment. At this point, the covering factor will decrease and the absorption will vanish (which would explain why no absorbers are seen in the haloes of radio galaxies with jet activity  $> 50 \text{ kpc}$  scales; Röttgering & Pentericci 1999). The Jeans mass in the shell will be of order  $10^6 M_{\odot}$  (Krause 2002). Hence the shell will fragment and form stars in globular clusters of this mass. Of course, at this point the shell should become visible in the rest-frame UV/optical as young stars form (which will also increase the ionization of the remaining parts of the shell). Assuming an efficiency of  $\sim 10$  per cent, this shell will contain a  $\sim 1000$  globular clusters of this mass – in reasonable agreement with the number of clusters found in nearby brightest cluster galaxies (Harris, Harris & McLaughlin 1998) which show excess of globular clusters systems compared to non-brightest cluster galaxies of comparable luminosity.

In summary, the most successful models of galaxy formation increasingly require outflows of gas to expel gas from galaxies at early times. In the most massive galaxies, most of the energy injection is believed to arise from the central AGN, making high-redshift radio galaxies, which have many of the characteristics expected for the progenitors of today’s massive ellipticals, strong candidates to empirically constrain the properties of outflows which can be used to test the models. The discovery of high-velocity ( $\sim 1000 \text{ km s}^{-1}$ ), halo-scale (i.e.  $\gg 150 \text{ kpc}$ ) and mass loaded winds in the vicinity of the central radio source is broadly in agreement with the requirements of models that invoke AGN-driven outflows to regulate star formation and black hole growth in luminous AGN (Di Matteo et al. 2005; Hopkins & Elvis 2010; Debuhr et al. 2012).

## ACKNOWLEDGEMENTS

We thank the referee for the constructive report on this paper and Yuichi Matsuda, Michele Fumagalli and Tom Theuns for useful discussions. We would also like to thank the pipeline developers for the data reduction package. AMS gratefully acknowledges an STFC Advanced Fellowship through grant number ST/H005234/1 and the Leverhulme foundation. IS acknowledges support from STFC (ST/I001573/1), the ERC Advanced Investigator programme DUSTYGAL 321334 and a Royal Society/Wolfson Merit Award. RB acknowledges support from the ERC advanced grant 339659-MUSICOS. BV acknowledges funding through ERC grant ‘Cosmic Dawn’. This publication uses data taken from the MUSE science verification programme 60.A-9318 and commissioning run 060.A-9100. All of the data used in this paper are available through the ESO science archive.

## REFERENCES

- Adam G., Rocca-Volmerange B., Gerard S., Ferruit P., Bacon R., 1997, *A&A*, 326, 501
- Adams T. F., 1975, *ApJ*, 201, 350
- Adams J. J., Hill G. J., MacQueen P. J., 2009, *ApJ*, 694, 314
- Alexander D. M., Swinbank A. M., Smail I., McDerimid R., Nesvadba N. P. H., 2010, *MNRAS*, 402, 2211
- Benson A. J., Bower R. G., Frenk C. S., Lacey C. G., Baugh C. M., Cole S., 2003, *ApJ*, 599, 38
- Binette L., Kurk J. D., Villar-Martín M., Röttgering H. J. A., 2000, *A&A*, 356, 23
- Binette L., Wilman R. J., Villar-Martín M., Fosbury R. A. E., Jarvis M. J., Röttgering H. J. A., 2006, *A&A*, 459, 31
- Booth C. M., Schaye J., 2010, *MNRAS*, 405, L1
- Bothwell M. S. et al., 2013, *MNRAS*, 429, 3047
- Bower R. G. et al., 2004, *MNRAS*, 351, 63
- Bower R. G., Benson A. J., Malbon R., Helly J. C., Frenk C. S., Baugh C. M., Cole S., Lacey C. G., 2006, *MNRAS*, 370, 645
- Bower R. G., Benson A. J., Crain R. A., 2012, *MNRAS*, 422, 2816
- Cantalupo S., Arrigoni-Battaia F., Prochaska J. X., Hennawi J. F., Madau P., 2014, *Nature*, 506, 63
- Churazov E., Sazonov S., Sunyaev R., Forman W., Jones C., Böhringer H., 2005, *MNRAS*, 363, L91
- Croton D. J. et al., 2006, *MNRAS*, 365, 11
- De Breuck C., van Breugel W., Minniti D., Miley G., Röttgering H., Stanford S. A., Carilli C., 1999, *A&A*, 352, L51
- De Breuck C., van Breugel W., Stanford S. A., Röttgering H., Miley G., Stern D., 2002, *AJ*, 123, 637
- De Breuck C. et al., 2004, *A&A*, 424, 1
- Debuhr J., Quataert E., Ma C.-P., 2012, *MNRAS*, 420, 2221
- Dekel A. et al., 2009, *Nature*, 457, 451
- Dijkstra M., Haiman Z., Spaans M., 2006, *ApJ*, 649, 14
- Di Matteo T., Springel V., Hernquist L., 2005, *Nature*, 433, 604
- Drouart G. et al., 2014, *A&A*, 566, A53
- Emonts B. H. C. et al., 2014, *MNRAS*, 438, 2898
- Erb D. K., Steidel C. C., Shapley A. E., Pettini M., Reddy N. A., Adelberger K. L., 2006, *ApJ*, 647, 128
- Fabian A. C., 1999, *MNRAS*, 308, L39
- Fardal M. A., Katz N., Gardner J. P., Hernquist L., Weinberg D. H., Davé R., 2001, *ApJ*, 562, 605
- Fechner C., Reimers D., 2007, *A&A*, 461, 847
- Gabor J. M., Davé R., Oppenheimer B. D., Finlator K., 2011, *MNRAS*, 417, 2676
- Geach J. E. et al., 2009, *ApJ*, 700, 1
- Genzel R. et al., 2014, *ApJ*, 796, 7
- Granato G. L., De Zotti G., Silva L., Bressan A., Danese L., 2004, *ApJ*, 600, 580
- Harris W. E., Harris G. L. H., McLaughlin D. E., 1998, *AJ*, 115, 1801
- Harrison C. M. et al., 2012, *MNRAS*, 426, 1073
- Harrison C. M., Alexander D. M., Mullaney J. R., Swinbank A. M., 2014, *MNRAS*, 441, 3306
- Hippelein H., Meisenheimer K., 1993, *Nature*, 362, 224
- Hopkins P. F., Elvis M., 2010, *MNRAS*, 401, 7
- Hopkins P. F., Hernquist L., Cox T. J., Robertson B., Springel V., 2006, *ApJS*, 163, 50
- Hopkins P. F., Cox T. J., Kereš D., Hernquist L., 2008, *ApJS*, 175, 390
- Hopkins P. F., Kereš D., Murray N., Hernquist L., Narayanan D., Hayward C. C., 2013, *MNRAS*, 433, 78
- Humphrey A., Villar-Martín M., Fosbury R., Binette L., Vernet J., De Breuck C., di Serego Alighieri S., 2007, *MNRAS*, 375, 705
- Humphrey A., Iwamuro F., Villar-Martín M., Binette L., Sung E. C., 2009, *MNRAS*, 399, L34
- Krause M., 2002, *A&A*, 386, L1
- Krause M., 2005, *A&A*, 436, 845
- Lagos C. D. P., Cora S. A., Padilla N. D., 2008, *MNRAS*, 388, 587
- McCarthy P. J., Spinrad H., Dickinson M., van Breugel W., Liebert J., Djorgovski S., Eisenhardt P., 1990, *ApJ*, 365, 487
- McCarthy P. J., van Breugel W., Kapahi V. K., 1991, *ApJ*, 371, 478
- McCarthy I. G., Schaye J., Bower R. G., Ponman T. J., Booth C. M., Dalla Vecchia C., Springel V., 2011, *MNRAS*, 412, 1965
- McQuinn M., Oh S. P., Faucher-Giguère C.-A., 2011, *ApJ*, 743, 82
- Magnelli B. et al., 2012, *A&A*, 539, A155
- Martin C. L., Shapley A. E., Coil A. L., Kornei K. A., Bundy K., Weiner B. J., Noeske K. G., Schiminovich D., 2012, *ApJ*, 760, 127
- Martin D. C., Chang D., Matuszewski M., Morrissey P., Rahman S., Moore A., Steidel C. C., Matsuda Y., 2014, *ApJ*, 786, 107
- Matsuda Y., Yamada T., Hayashino T., Yamauchi R., Nakamura Y., 2006, *ApJ*, 640, L123
- Matsuda Y. et al., 2011, *MNRAS*, 410, L13
- Matsuda Y. et al., 2012, *MNRAS*, 425, 878
- Miley G., De Breuck C., 2008, *A&AR*, 15, 67
- Miley G. K. et al., 2004, *Nature*, 427, 47
- Navarro J. F., Frenk C. S., White S. D. M., 1997, *ApJ*, 490, 493
- Nelan J. E., Smith R. J., Hudson M. J., Wegner G. A., Lucey J. R., Moore S. A. W., Quinney S. J., Suntzeff N. B., 2005, *ApJ*, 632, 137
- Nesvadba N. P. H., Lehnert M. D., De Breuck C., Gilbert A., van Breugel W., 2007, *A&A*, 475, 145
- Newman S. F. et al., 2012, *ApJ*, 761, 43
- Nilsson K. K., Fynbo J. P. U., Møller P., Sommer-Larsen J., Ledoux C., 2006, *A&A*, 452, L23
- Ohyama Y., Taniguchi Y., 2004, *AJ*, 127, 1313
- Pettini M., Rix S. A., Steidel C. C., Hunt M. P., Shapley A. E., Adelberger K. L., 2002, *Ap&SS*, 281, 461
- Röttgering H., Pentericci L., 1999, in Röttgering H. J. A., Best P. N., Lehnert M. D., eds, *The Most Distant Radio Galaxies*. Royal Netherlands Academy of Arts and Sciences (KNAW), Amsterdam, p. 85
- Röttgering H. J. A., Hunstead R. W., Miley G. K., van Ojik R., Wieringa M. H., 1995, *MNRAS*, 277, 389
- Sánchez S. F., Humphrey A., 2009, *A&A*, 495, 471
- Schaye J., Theuns T., Rauch M., Efstathiou G., Sargent W. L. W., 2000, *MNRAS*, 318, 817
- Silk J., Rees M. J., 1998, *A&A*, 331, L1
- Smail I., Blundell K. M., 2013, *MNRAS*, 434, 3246
- Springel V., Hernquist L., 2003, *MNRAS*, 339, 312
- Springel V., Di Matteo T., Hernquist L., 2005, *MNRAS*, 361, 776
- Steidel C. C., Erb D. K., Shapley A. E., Pettini M., Reddy N., Bogosavljević M., Rudie G. C., Rakic O., 2010, *ApJ*, 717, 289
- Swinbank A. M., Bower R. G., Smith G. P., Wilman R. J., Smail I., Ellis R. S., Morris S. L., Kneib J.-P., 2007, *MNRAS*, 376, 479
- Swinbank A. M. et al., 2009, *MNRAS*, 400, 1121
- Swinbank A. M. et al., 2014, *MNRAS*, 438, 1267
- Tadhunter C. N., Villar-Martín M., Morganti R., Bland-Hawthorn J., Axon D., 2000, *MNRAS*, 314, 849
- Taniguchi Y., Shioya Y., Kakazu Y., 2001, *ApJ*, 562, L15
- van Breugel W. J. M., Stanford S. A., Spinrad H., Stern D., Graham J. R., 1998, *ApJ*, 502, 614

- van Ojik R., Roettgering H. J. A., Carilli C. L., Miley G. K., Bremer M. N., Macchetto F., 1996, *A&A*, 313, 25
- van Ojik R., Roettgering H. J. A., Miley G. K., Hunstead R. W., 1997, *A&A*, 317, 358
- Venemans B. P. et al., 2002, *ApJ*, 569, L11
- Venemans B. P. et al., 2007, *A&A*, 461, 823
- Villar-Martín M., Vernet J., di Serego Alighieri S., Fosbury R., Humphrey A., Pentericci L., 2003, *MNRAS*, 346, 273
- Villar-Martín M., Humphrey A., De Breuck C., Fosbury R., Binette L., Vernet J., 2007a, *MNRAS*, 375, 1299
- Villar-Martín M., Sánchez S. F., Humphrey A., Dijkstra M., di Serego Alighieri S., De Breuck C., González Delgado R., 2007b, *MNRAS*, 378, 416
- Weijmans A.-M., Bower R. G., Geach J. E., Swinbank A. M., Wilman R. J., de Zeeuw P. T., Morris S. L., 2010, *MNRAS*, 402, 2245
- Weilbacher P. M., Streicher O., Urrutia T., Pécontal-Rousset A., Jarno A., Bacon R., 2014, in Manset N., Forshay P., eds, *ASP Conf. Ser. Vol. 485, Astronomical Data Analysis Software and Systems XXIII*. Astron. Soc. Pac., San Francisco, p. 451
- Weingartner J. C., Draine B. T., 2001, *ApJ*, 548, 296
- Wilman R. J., Jarvis M. J., Röttgering H. J. A., Binette L., 2004, *MNRAS*, 351, 1109
- Wilman R. J., Gerssen J., Bower R. G., Morris S. L., Bacon R., de Zeeuw P. T., Davies R. L., 2005, *Nature*, 436, 227
- Yang Y., Zabludoff A., Jahnke K., Eisenstein D., Davé R., Shectman S. A., Kelson D. D., 2011, *ApJ*, 735, 87
- Yang Y., Zabludoff A., Jahnke K., Davé R., 2014, *ApJ*, 793, 114

This paper has been typeset from a  $\text{\TeX}/\text{\LaTeX}$  file prepared by the author.